Parallel Solution of 3D Ohta-Kawasaki Nonlocal Phase Field Model in FEniCS

Gabriel F. Barros[1], Adriano M. A. Côrtes[2], Alvaro L. G. A. Coutinho[1]

[1]*Civil Engineering, COPPE/Federal University of Rio de Janeiro*
Rio de Janeiro, RJ 21941-598, Brazil
gabriel.barros@nacad.ufrj.br, alvaro@nacad.ufrj.br
[2]*NUMPEX-COMP, Federal University of Rio de Janeiro*
Duque de Caxias, RJ 25240-005, Brazil
adriano@nacad.ufrj.br

Abstract. This study presents new results for the parallel solution of the 3D nonlocal Cahn-Hilliard equation derived from the Ohta-Kawasaki free energy functional with adaptive time step control. The temporal adaptivity scheme is recast under the linear feedback control theory equipped with an error estimation that extrapolates the solution obtained from an energy-stable, fully implicit time marching scheme. We use three time-step controllers with different properties: a simple Integral controller, a complete Proportional-Integral-Derivative controller, and the PC11 predictive controller. We explore how different controllers affect the convergence of the nonlinear solver for two values of the nonlocal parameter. The efficiency of the adaptive schemes for the nonlocal Cahn-Hilliard equation is evaluated in terms of the number of time steps required for the complete simulation and the computational effort measured by the required number of nonlinear and linear solver iterations. We show numerical evidence of mass conservation and free energy decay for both nonlocal parameters.

Keywords: Nonlocal Cahn-Hilliard equation, Time step size adaptivity, Ohta-Kawasaki Functional, Feedback Control Theory

1 Introduction

The numerical simulation of the Cahn-Hilliard (CH) equation is important in many different scientific and engineering fields. It was first derived in 1958 to model the phase separation in binary alloys [1, 2] and, since then, the CH equation appears in several different physical contexts [3] such as diblock copolymers, image inpainting, binary fluid flow, fracture propagation, and topology optimization. For the specific case of the diblock copolymers, a nonlocal version of the CH equation is often considered since the nature of this physics relies on long-range interactions compared to the usual short-range interactions modeled by the standard CH equation.

This study is an extension of [4], in which the use of temporal adaptivity schemes within the linear feedback control theory was evaluated on both CH and Nonlocal Cahn-Hilliard (NCH) equations. Here, we focus on the NCH equation, where an additional term is added to the CH equation responsible for modeling the long-range interactions between phases. We consider the finite element method for spatial discretization and an energy unconditional stable method for temporal discretization. We also evaluate three different time step size adaptivity schemes within the linear feedback control strategy to improve the efficiency of our simulations. In [4], we compared two 3D NCH simulations with the same nonlocal term and different monomer proportions, while in the present study, we preserve the ratio between phases while comparing the effects of using different nonlocal parameters.

2 Governing Equations

We consider the following nonlocal extension of the standard CH equation, that is, the NCH equation,

$$\frac{\partial \phi}{\partial t} = \nabla \cdot \left[M(\phi) \nabla \left(\frac{\partial \Psi}{\partial \phi} - \epsilon^2 \Delta \phi \right) \right] - \sigma(\phi - \bar{\phi}), \tag{1}$$

where σ represents the nonlocal parameter, responsible for modeling the magnitude of the long-range microforces between the phases. The parameter $\bar{\phi}$ is the mean value of ϕ in the domain $\Omega \in \mathrm{R}^{n_{sd}}$ with boundary $\partial\Omega$ and $n_{sd} = 2, 3$. The NCH equation is derived from the O–K functional, that can be written [5, 6] as,

$$F(\phi) = \int_\Omega \left(\Psi(\phi) + \frac{\epsilon^2}{2} |\nabla \phi|^2 \right) d\Omega + \int_\Omega \frac{\sigma}{2} |\nabla v|^2 d\Omega, \tag{2}$$

where v is related to ϕ via the boundary value problem $-\Delta v = (\phi - \bar{\phi})$.

The O–K free energy functional is derived from the mean field theory in the context of diblock copolymers [7]. In the case where $\sigma = 0$, the O–K functional (2) becomes the Ginzburg-Landau free energy functional [8]. Consequently, in this case, the NCH equation (1) becomes the CH equation. Both CH [9], and NCH [10] equations minimize the interfaces between phases, solving the isoperimetric problem. The difference, however, lies in the fact that the Ginzburg-Landau free energy functional is minimized through the separation of phases due to short-range microforces while the O–K free energy functional models pattern morphologies via energy minimization involving the competition of both short and long-range microforces, where the latter is modeled by the magnitude of the nonlocal parameter σ. The competition between local and nonlocal microforces in the O–K free energy functional leads to many different pattern formations in the equilibrium configuration of a copolymer melt, such as lamellae, spheres, gyroids, and cylinders [6]. It is possible to map a given copolymer structure to a set of NCH parameters, such as ϵ, $\bar{\phi}$, and σ by a phase diagram [5, 6, 11] and the structure of the generated polymer is of utmost importance on several applications in science and engineering such as nanotechnology and materials science [6].

3 Numerical Methodology

In this study, we evaluate the performance and accuracy of three different time step adaptivity schemes on the numerical solution of the NCH. The finite element method is employed to discretize in space the NCH equation. Since the NCH is a fourth-order PDE, standard C^0-continuous finite elements are not suitable. Nonetheless, there are other approaches, such as isogeometric analysis [12], discontinuous Galerkin [13], and C^1-continuous elements [14]. However, we consider the splitting approach [15], where the fourth-order PDE can be solved as a nonlinear system of two second-order PDEs, thus enabling the use of C^0-continuous finite elements at the cost of an extra degree of freedom per node. As for the temporal integration, we consider an implicit, second-order, unconditionally energy-stable method originally proposed for the CH equation and other traditional phase-field equations [16]. This method enables the use of larger time steps obtained by time adaptivity without affecting the numerical stability of the simulations. As for the temporal adaptivity schemes, the error is estimated *a posteriori* by extrapolation by a lower-order time integration method in comparison with the temporal integration method [16]. Since the integration method of our choice is second-order, the extrapolation is done by the backward-Euler method, a first-order approach. This error estimation strategy is efficient since it avoids the necessity of computing the solution at the same instant for multiple time integration methods of different orders (i.e., see [9, 12, 17]). With the error estimated, we consider three different controllers (Integral, Predictive, and Proportional-Integral-Derivative) responsible for generating time step sizes able to keep the errors within a given tolerance. If the error is larger than a given threshold, the time step size is recomputed, and the solution for that instant is rejected. We evaluate the results in terms of mass conservation and free energy decay. All the numerical solutions are computed using the `FEniCS` framework version 2019.1.0 [18], a high-performance finite element library written in Python/C++, using 24 cores. For further detailed information regarding the implementation and numerical aspects of the simulations, we encourage the readers to read our previous work [4].

4 Numerical Experiments

In this section, we present the results of our numerical experiments. Our simulations consist of the resolution of the NCH on a cubic domain with 129^3 nodes, 128^3 equally spaced cells, each cell subdivided into 6 tetrahedral finite elements. We show the results for $\sigma = 500$ and $\sigma = 750$. Other physical parameters such as the interface parameter $\epsilon = 0.1$ and $\bar{\phi} = 0.0$ are kept identical for both simulations and the simulations start with an initial time step size of $\Delta t_0 = 1 \times 10^{-9}$. Initially, we discuss the time step size histories shown in Figure 1. We can analyze this figure by splitting the simulation time into three stages: an initial stage with a fast time step-growth, an intermediate stage, where the time step increases but oscillates, and the final stage where the time step recovers a fast growth.

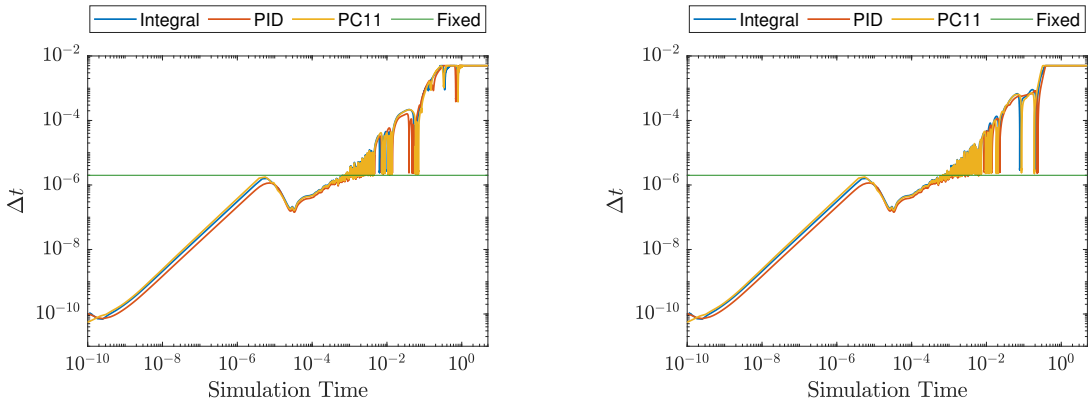

Figure 1. Time step size history for the three controllers. Left, $\sigma = 500$; right, $\sigma = 750$.

For the initial stage, we observe that the simulation starts with a time step size around 10^{-10}. This means that the solutions obtained using the initial time step size prescribed as Δt_0 are too large to be kept within the prescribed tolerances. The controllers are responsible for adjusting the time step sizes to fit this criterion. We also observe an increase in the time step size in terms of orders of magnitude, meaning that after the initial time steps, the time step size is too small for the physics. As for the intermediate stage, we observe some oscillations on the time step size related to the physical aspects of the copolymer. The dynamics become more rapid when bubbles shrink, requiring the time step size to diminish, and, after the occurrence of this phenomenon, the dynamics become slower, allowing the time step size to increase. This occurs multiple times for each bubble under the effect of Ostwald's ripening phenomena, leading to the time step size oscillation observed in the intermediate stage. This leads to the final stage, where time step sizes are large enough to track the interface motion. Comparing the graphs in Figure 1, we note some differences. For $\sigma = 500$, we observe some minor differences among the curves for the three controllers, while for $\sigma = 750$, the curves are practically overlapping. This indicates that, despite leading to the formation of identical melts, the use of different time step size controllers for the numerical solution of the NCH equation may lead to different temporal trajectories until reaching the steady-state. This affects the dynamical evolution in the sense that the same physical phenomena are observed in different simulation times [4]. However, being the copolymer melt the most important information in NCH simulations, the difference between the time step curves is negligible. For the case where $\sigma = 750$, the three curves reveal similar behavior as observed on the simulations for the CH equation on [4]. The copolymer melts can be seen in Figs. 2 and 3 for $\sigma = 500$ and $\sigma = 750$ respectively. The figures show the evolution of copolymer melts at the different transient stages and the steady-state, showing that the chosen parameters lead to stable melts.

Table 1 shows the performance data for the simulated cases. We notice that the I controller presents a larger number of rejected steps, while the PID has a larger number of total time steps (accepted and rejected), while the PC11 yielded the smallest number of total time steps. Despite being a good metric for efficiency, the time step controller has a significant influence on the solver requiring thus evaluating the total number of linear and nonlinear iterations. For the I controller and $\sigma = 750$, the average number of linear iterations is larger than the other cases. We observe that the PC11 controller yields better performance when $\sigma = 500$ and the PID controller is the most efficient controller for the case where $\sigma = 750$. In terms of accuracy, we observe the free energy decay and mass conservation properties in Fig. 4 for the best performing controllers for each case. Mass conservation is within the accuracy obtained at each time step solve, and the free energy decreases monotonically for both cases.

5 Conclusions

In this study, we present new results for the solution of the NCH using different controllers for the temporal adaptivity scheme. This paper is an extension of our previous work where we studied the efficiency of the use of time step size controllers on diblock copolymer simulations [4]. This study compares the results for two 3D copolymer melts with different nonlocal parameters σ. We observe that the time step size curve for the three proposed controllers is affected by σ in the sense that, for $\sigma = 500$, the curves for the three controllers are different, while for $\sigma = 750$, the three curves are practically identical. In both cases, the copolymer structure is different due to the difference between the nonlocal parameter, although the melts obtained are identical for the three controllers. We also evaluate the physical quantities of interest, such as mass and free energy of the system, and confirmed mass conservation and free energy decay as expected. Finally, we evaluated the results in

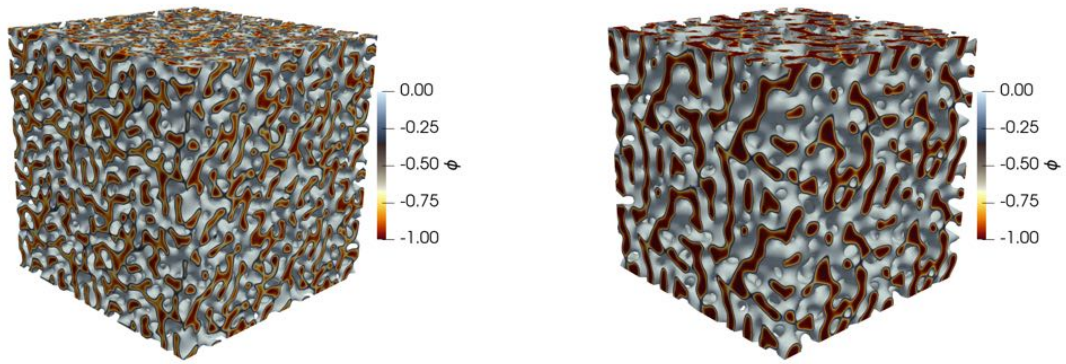

a) $t = 9.60 \times 10^{-5}$ b) $t = 3.24 \times 10^{-4}$

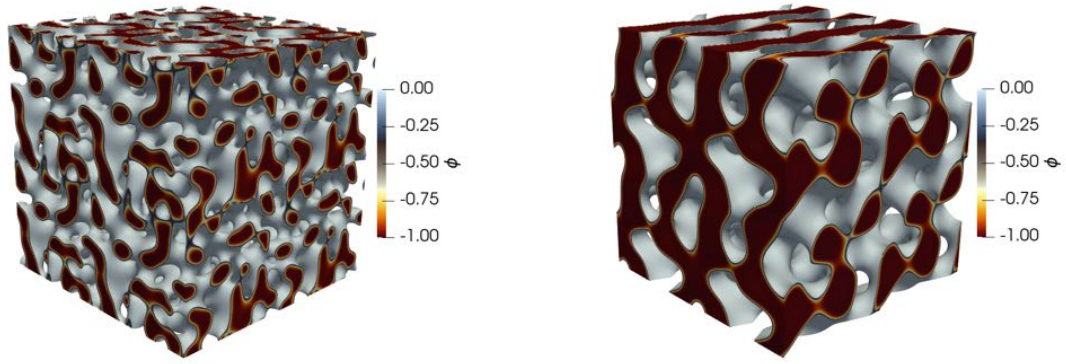

c) $t = 7.49 \times 10^{-4}$ d) $t = 7.52 \times 10^{-3}$

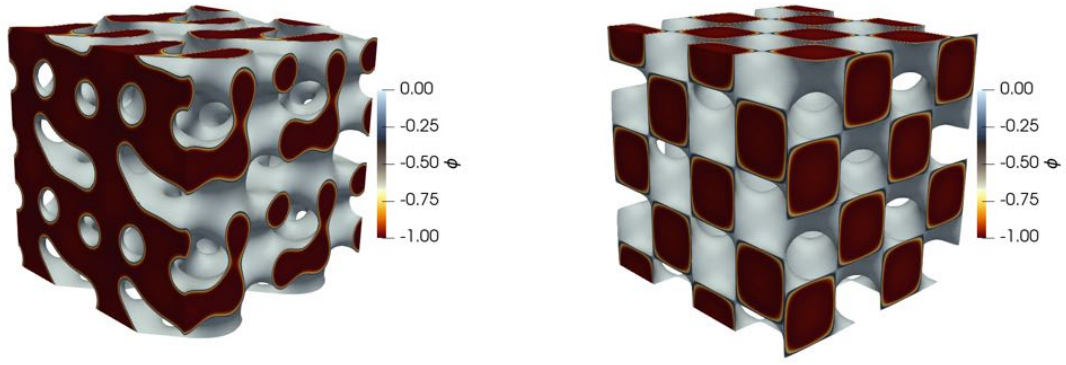

e) $t = 4.22 \times 10^{-2}$ f) $t = 1.11 \times 10^{0}$

Figure 2. Evolution in time and final structure of a monomer on the generated diblock copolymer melts from the 3D simulations for $\sigma = 500$.

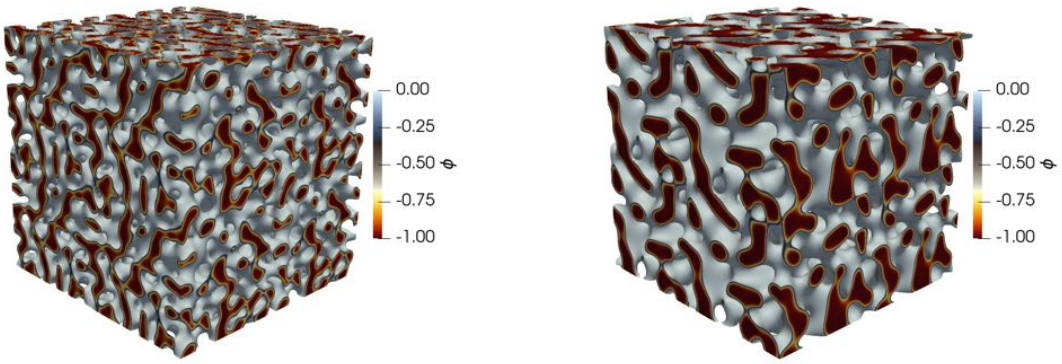

a) $t = 2.46 \times 10^{-4}$ b) $t = 1.05 \times 10^{-3}$

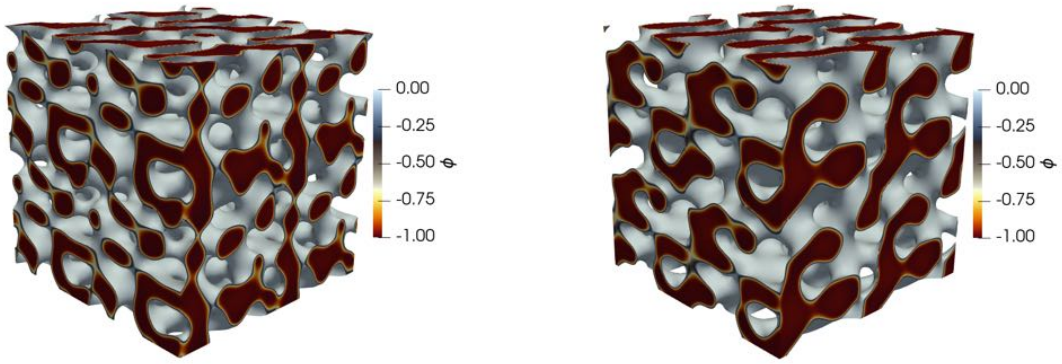

c) $t = 6.19 \times 10^{-3}$ d) $t = 2.15 \times 10^{-2}$

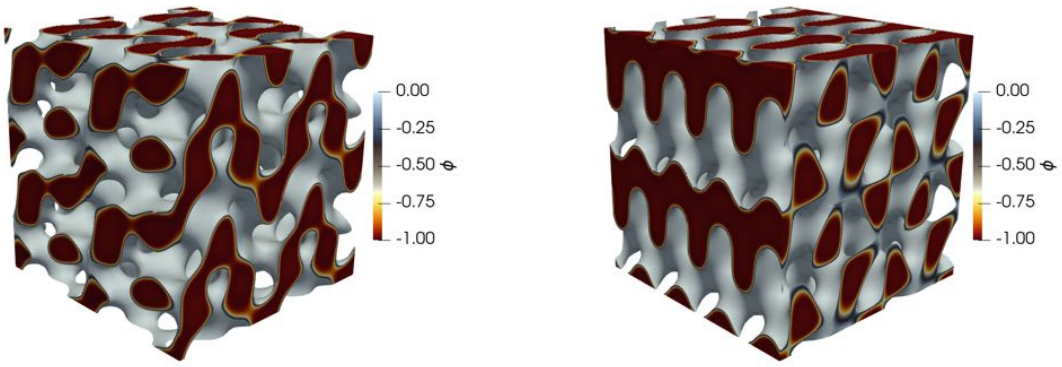

e) $t = 1.70 \times 10^{-1}$ f) $t = 0.18 \times 10^{0}$

Figure 3. Evolution in time and final structure of a monomer on the generated diblock copolymer melts from the 3D simulations for $\sigma = 750$.

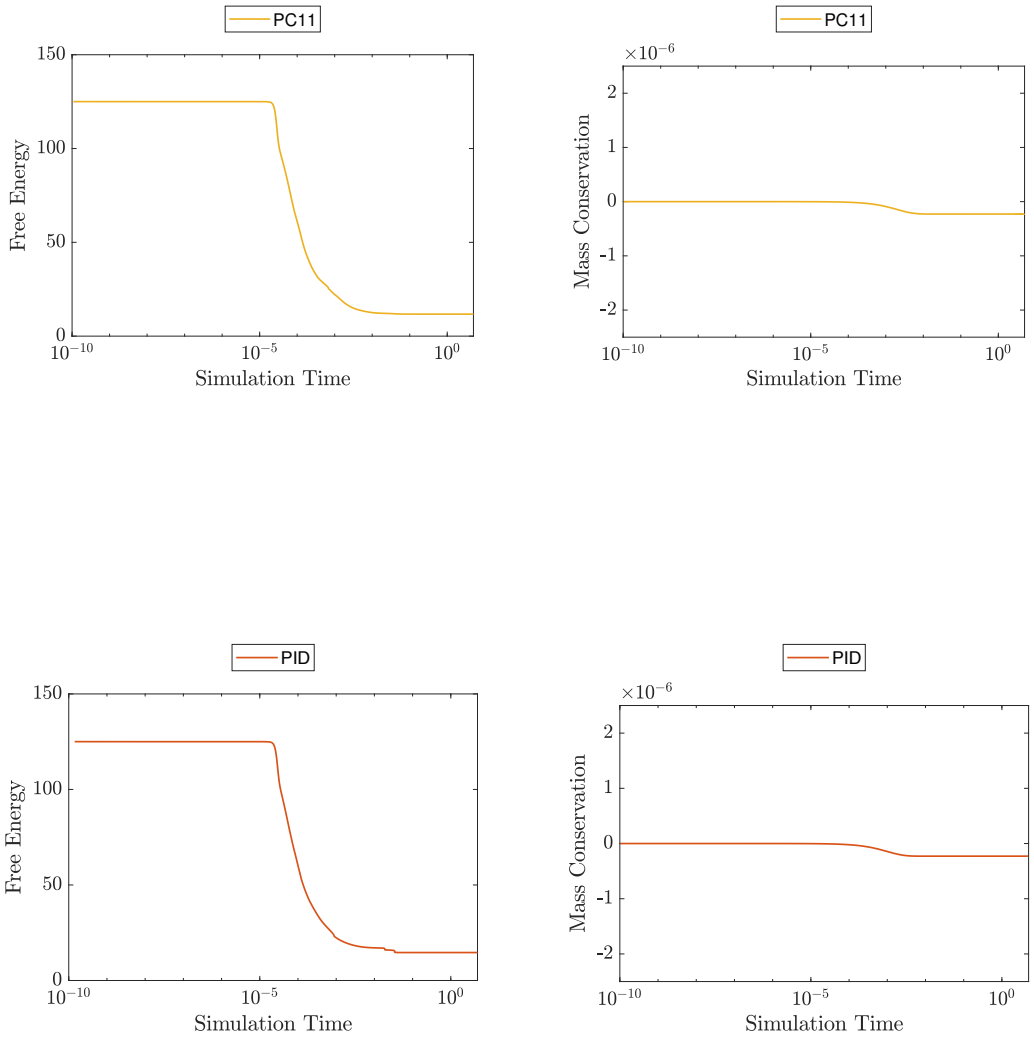

Figure 4. Free energy and mass conservation for the 3D simulations for the best performing controllers. Top $\sigma = 500$; bottom, $\sigma = 750$.

Table 1. Results for the time adaptivity schemes for each time step controller in the 3D diblock copolymer simulations.

σ	Time Step Controller	Accepted Steps	Rejected Steps	Avg. Nonlinear Iterations	Avg. Linear Iterations	Relative CPU Effort
500	I	4339	313	7.5168	722.6998	1.00
	PID	5017	157	7.1780	607.4357	0.95
	PC11	4481	47	6.8601	593.4483	0.79
750	I	4203	286	7.9892	1037.7831	1.00
	PID	4789	157	6.8434	502.5649	0.55
	PC11	4354	37	6.8202	613.4493	0.57

terms of efficiency by crossing the information obtained by the adaptivity schemes (such as the number of time steps computed) with the solver information (linear and nonlinear iterations). The PC11 controller and the PID controller yielded better results for the cases where $\sigma = 500$ and $\sigma = 750$, respectively. The use of the most efficient controllers in each case revealed the efficiency of 21% and 45%, respectively.

Acknowledgements. This work is funded by CNPq and FAPERJ. Gabriel F. Barros is supported by the Coordenação de Aperfeiçoamento de Pessoal de Nível Superior - Brasil (CAPES) - Finance Code 001. Computer time in Lobo Carneiro supercomputer is provided by the High-Performance Computing Center of COPPE/UFRJ.

Authorship statement. This section is mandatory and should be positioned immediately before the References section. The text should be exactly as follows: The authors hereby confirm that they are the sole liable persons responsible for the authorship of this work, and that all material that has been herein included as part of the present paper is either the property (and authorship) of the authors, or has the permission of the owners to be included here.

References

[1] J. W. Cahn and J. E. Hilliard. Free energy of a nonuniform system. i. Interfacial Free Energy. *The Journal of Chemical Physics*, vol. 28, n. 2, pp. 258–267, 1958a.
[2] J. W. Cahn and J. E. Hilliard. Free energy of a nonuniform system. ii. Thermodynamic Basis. *The Journal of Chemical Physics*, vol. 30, n. 5, pp. 1121–1124, 1958b.
[3] J. Kim, S. Lee, Y. Choi, S. Lee, and D. Jeong. Basic Principles and Practical Applications of the Cahn-Hilliard Equation. *Mathematical Problems in Engineering*, vol. , n. ID 9532608, pp. 1–11, 2016.
[4] G. F. Barros, A. M. A. Côrtes, and A. L. G. A. Coutinho. Finite element solution of nonlocal Cahn–Hilliard equations with feedback control time step size adaptivity. *International Journal for Numerical Methods in Engineering*, vol. Early View, 2021.
[5] J. B. Van den Berg and J. F. Williams. Validation of the bifurcation diagram in the 2D Ohta-Kawasaki problem. *Nonlinearity*, vol. 30, n. 4, pp. 1584–1638, 2017.
[6] R. Choksi, M. A. Peletier, and J. F. Williams. On the Phase Diagram for Microphase Separation of Diblock Copolymers: An Approach via a Nonlocal Cahn-Hilliard Functional. *SIAM Journal on Applied Mathematics*, vol. 69, n. 6, pp. 1712—-1738, 2009.
[7] T. Ohta and K. Kawasaki. Equilibrium Morfology of Block Copolymer Melts. *Macromolecules*, vol. 19, n. 10, pp. 2621–2632, 1986.
[8] H. Gomez and K. G. van der Zee. Encyclopedia of computational mechanics second edition. *Computational Phase-Field Modeling*, vol. , pp. 1–35, 2017.
[9] O. Wodo and B. Ganapathysubramanian. Computationally efficient solution to the Cahn-Hilliard equation: Adaptive implicit time schemes, mesh sensitivity analysis and the 3D isoperimetric problem. *Journal of Computational Physics*, vol. 230, n. 15, pp. 6037–6060, 2011.
[10] R. Choksi. Nonlocal Cahn–Hilliard and isoperimetric problems: Periodic phase separation induced by competing long- and short-term interactions. *CRM Proceedings and Lecture Notes: Singularities in PDE and the Calculus of Variations, American Math. Society*, vol. , pp. 33–45, 2006.
[11] R. Choksi, M. Maras, and J. F. Williams. 2D phase diagram for minimizers of a Cahn-Hilliard functional with long-range interactions. *SIAM Journal on Applied Dynamical Systems*, vol. 10, n. 4, pp. 1344–1362, 2011.
[12] H. Gómez, V. M. Calo, Y. Bazilevs, and T. J. R. Hughes. Isogeometric analysis of the Cahn-Hilliard phase-field model. *Computer Methods in Applied Mechanics and Engineering*, vol. 197, n. 49-50, pp. 4333–4352, 2008.
[13] G. N. Wells, E. Kuhl, and K. Garikipati. A discontinuous Galerkin method for the Cahn-Hilliard equation. *Journal of Computational Physics*, vol. 218, n. 2, pp. 860–877, 2006.
[14] R. H. Stogner, G. F. Carey, and B. T. Murray. Approximation of Cahn-Hilliard diffuse interface models using parallel adaptive mesh refinement and coarsening with C1 elements. *International Journal for Numerical Methods in Engineering*, vol. 76, n. 5, pp. 636–661, 2008.
[15] C. M. Elliot, D. A. French, and F. A. Milner. A second order splitting method for the Cahn-Hilliard equation. *Numerische Mathematik*, vol. 54, n. 5, pp. 575–590, 1989.
[16] P. Vignal, N. Collier, L. Dalcin, D. L. Brown, and V. M. Calo. An energy-stable time-integrator for phase-field models. *Computer Methods in Applied Mechanics and Engineering*, vol. 316, pp. 1179–1214, 2017.
[17] L. Cueto-Felgueroso and J. Peraire. A time-adaptive finite volume method for the Cahn-Hilliard and Kuramoto-Sivashinsky equations. *Journal of Computational Physics*, vol. 227, n. 24, pp. 9985–10017, 2008.
[18] M. S. Alnæs, J. Blechta, J. Hake, A. Johansson, B. Kehlet, A. Logg, C. Richardson, J. Ring, M. E. Rognes, and G. N. Wells. The FEniCS Project Version 1.5. *Archive of Numerical Software*, vol. 3, n. 100, 2015.